Limnol. Oceanogr., 46(2), 2001, 368–380

Nitrogen isotopic evidence for micronutrient control of fractional NO_3^- utilization in the equatorial Pacific

Mark A. Altabet
School for Marine Science and Technology, University of Massachusetts–Dartmouth, New Bedford, Massachusetts 02744

Abstract

During the U.S. JGOFS EqPac program, variations in nitrogen isotopic ratio ($\delta^{15}N$) and their control by relative NO_3^- drawdown were examined in detail. Near-surface $\delta^{15}NO_3^-$ data clearly conform to Rayleigh isotopic fractionation during phytoplankton utilization of NO_3^-, with a fractionation factor of about 5‰. This isotopic signal both propagates into particulate nitrogen pools and is a persistent, large-scale characteristic of the system. Decreasing near-surface [NO_3^-] with distance from the equator strongly correlates with increasing $\delta^{15}N$ in euphotic zone particulate organic matter (POM) as well as sinking particles during both Surveys 1 (El Niño) and 2 (non–El Niño) cruises. Despite a doubling of [NO_3^-] accompanying relaxation of El Niño conditions, $\delta^{15}N$ values in near-surface POM and deeply sinking particles as a function of latitude were similar for the two periods. Since $\delta^{15}N$ varies with relative nutrient drawdown and not its concentration, this parameter appears to not have varied significantly. In both cases, about 50% of upwelled NO_3^- was consumed in the immediate vicinity of the equator, as estimated from the $\delta^{15}N$ data. The moored sediment trap time series provided a more highly resolved temporal view of the ^{15}N dynamics of this system. At the equator and to the south, there is little temporal variation in $\delta^{15}N$ and, hence, in relative NO_3^- utilization over the 1-yr duration of the program. At 2° and 5°N, there is a large 5‰ decrease in $\delta^{15}N$ during the transition to non–El Niño conditions in response to the northward movement of NO_3^--rich waters, which probably reflects the intensification of the north equatorial current. Overall, % NO_3^- utilization at the equator remained between 40 and 60% over the observation period, despite large hydrographic and dynamical changes. This observation implies a tight control of relative NO_3^- utilization, consistent with iron (Fe) limitation. Since Fe is supplied in this region by upwelling, relative NO_3^- utilization is likely determined by the product of the ratio of Fe to NO_3^- in upwelled waters and the NO_3^- : Fe utilization ratio. Given no change in the chemistry of source waters, increases in upwelling, as observed during the transition away from El Niño, will affect surface [NO_3^-] new and export production, but it will not affect relative NO_3^- utilization. In this light, downcore $\delta^{15}N$ records in the equatorial Pacific should reflect past changes in the limitation of NO_3^- drawdown by Fe, perhaps through changes in equatorial undercurrent chemistry.

The equatorial Pacific is one of the Pacific Ocean's three major high nutrient–low chlorophyll (HNLC) regions. It is distinguished by persistent equatorial upwelling, and this dominant source of new macronutrients (nitrogen [N], phosphorus [P], and silicon [Si]) to the euphotic zone (e.g., Wyrtki 1981; Chavez and Barber 1987) accounts for this region's moderately high productivity and export flux (Peña et al. 1992; Honjo et al. 1995; McCarthy et al. 1995; Landry et al. 1997). Poleward advection of upwelled waters (as well as advection to the west) combined with progressive nutrient drawdown produces large-scale gradients in near-surface [NO_3^-] and [PO_4^{-3}]. Limitation of export production by iron (Fe) availability shapes these gradients by preventing macronutrient depletion in the immediate vicinity of the equator (Kolber et al. 1994; Martin et al. 1994; Chai et al. 1996; Coale et al. 1996; Landry et al. 1997). Si limitation of diatom production and efficient nutrient recycling have also both been implicated in creating HNLC conditions (Ku et al. 1995; Dugdale and Wilkerson 1998). Temporal variability occurs at a variety of scales but most notably those of El Niño (ENSO). During ENSO events, disruption of the large-scale circulation of the equatorial Pacific combined with reduction of upwelling winds reduces nutrient flux to surface waters as well as productivity.

It has been previously demonstrated that the poleward gradients in macronutrients are negatively correlated with particulate organic matter (POM) nitrogen isotopic ratio ($\delta^{15}N$ in ‰ units relative to atmospheric N_2; Altabet and Francois 1994*a*,*b*; Altabet 1996). These large-scale variations in $\delta^{15}N$ result from isotopic fractionation during phytoplankton NO_3^- uptake. This effect has been demonstrated in numerous laboratory (Wada and Hattori 1978; Montoya and McCarthy 1995; Pennock et al. 1996; Waser et al. 1998) and field (Altabet and Deuser 1985; Altabet 1989; Goering et al. 1990; Altabet et al. 1991; Nakatsuka et al. 1991; Altabet 1996; Sigman et al. 1997; Altabet et al. 1999) studies. The relationship between the NO_3^- utilization and the $\delta^{15}N$ of NO_3^- ($\delta^{15}NO_3^-$) has been shown in several of these studies to conform to Rayleigh fractionation ($\delta^{15}NO_3^-$ increased exponentially with decreasing [NO_3^-]). These isotopic signals were found to propagate down the water column from sinking particles to core-top sediments along 140°W (Altabet and Francois 1994*a*,*b*). Farrell et al. (1995) extended this work

Acknowledgments

This work was funded by NSF grants OCE-9115641 and OCE-9526356. Paula Prayzner, Rehka Singh, David Galthier, and Xinqun Huang provided technical assistance. James J. McCarthy and John Nevins kindly provided water-column samples (NSF OCE-9022411). Susumo Honjo and Steve Manganini from WHOI (NSF OCE 9022365) and Jack Dymond and Robert Collier from OSU (NSF OCE 9022316) provided sediment trap material. Craig Smith provided sea-floor ''fluff'' material (NSF OCE-9022408). Steve Carey provided sediment core material from the URI core library (NSF OCE-9102410). Alan Mix provided the PC72 age model and foraminiferal $\delta^{18}O$ data. This is University of Massachusetts SMAST contribution 990602.

by showing that seafloor sediment $\delta^{15}N$ is inversely related to surface NO_3^- concentration when mapped both meridionally and zonally over a large region of the eastern equatorial Pacific. Their downcore, paleoceanographic data were interpreted as reflecting reduced fractional utilization of NO_3^- during the last glacial maximum in response to increased upwelling intensity.

Here a detailed analysis of the systematics and significance of nitrogen isotopic signals observed during the U.S. JGOFS EqPac program is presented. Carbon/nitrogen and $\delta^{13}C$ data are also presented in considering the source of sinking particles. The sampling periods straddled the relaxation of ENSO to more normal conditions, giving us the opportunity to use the $\delta^{15}N$ data to study the transitions in biogeochemistry that occurred during this period. The relative constancy of $\delta^{15}N$ values at the equator is surprising since there was a doubling of near-surface NO_3^- concentration with increased upwelling intensity. This phenomenon is explained in terms of maintenance of near-constant fractional utilization of upwelled NO_3^- resulting from Fe limitation of NO_3^- utilization. These results not only have consequences for understanding the modern equatorial Pacific but also for the interpretation of paleoceanographic data.

Sampling and analytical methods

Water column sampling—Near-surface waters were sampled during both the EqPac Survey 1 (S1; March 1992) and Survey 2 (S2; August 1992) cruises. Stations were generally along 140°W and between 9°N and 12°S. As reported previously (Murray et al. 1995), these observational periods corresponded to ENSO (El Niño) and more normal conditions, respectively. Corresponding contrasts in plankton dynamics and biogeochemistry were observed, including large changes in near-surface nutrient concentration. Underway samples were collected on each cruise from the ship's uncontaminated seawater line with suspended POM collected onto precombusted 29.3-cm Whatman GF/F filters. Pressure was maintained at between 5 and 10 PSI. Water column samples were collected using Niskin bottles with POM pressure filtered onto precombusted 4.7-cm Whatman GF/F filters, also at 5–10 PSI. Water samples for $\delta^{15}NO_3^-$ analysis were taken from filtrate and frozen for later analysis. NO_3^- concentration data were provided by C. Garside and are available in the U.S. JGOFS database (http://www1.whoi.edu/jg/dir/jgofs/eqpac/).

Sediment trap and fluff sampling—Mark VI time-series sediment traps (0.5 m^2 collection area) were deployed in January 1992 for the 1-yr period spanning the U.S. JGOFS EqPac Program (Honjo et al. 1995). Mooring sites were located along or near 140°W, nominally at the latitudes of 9°N, 5°N, 2°N, 0°, 2°S, 5°S, and 12°S (Table 1). The 12°S mooring was placed at 135°W. Up to four Mark VI sediment traps were placed on each mooring at different depths to resolve possible vertical variations in particle flux and composition. All Mark VI traps were fitted with a rotating tray of 21 sample cups. Each trap was programmed to rotate simultaneously every 17 d, resulting in a synchronized time-series sample set. Sampling for the entire set of sediment traps commenced on 2 February 1992 and ended on 14 January 1993. Unfortunately, a number of traps experienced microprocessor failure and ended time-series sampling prematurely, though at least one complete time series was available for each site. Those locations and depths for which data is presented in this study are listed in Table 1.

Table 1. Summary of moored sediment trap locations, trap depths, bottom depth, and preservative used. This list pertains only to those samples analyzed for this study. Time-series data for the formalin-preserved sediment trap samples are found in Figs. 8–10. A comparison of the effects of the different preservatives used at 5°S is found in Fig. 1.

Designation	Latitude	Longitude	Bottom depth (m)	Trap depths (m)	Preservative
9°N	9°00′N	139°59′W	5,100	1,250	Formalin
				2,150	Formalin
				4,400	Formalin
5°N	5°01′N	139°47′W	4,493	1,191	Formalin
				2,193	Formalin
				3,793	Formalin
2°N	2°00′N	140°08′W	4,397	2,203	Formalin
0°	0°04′N	139°45′W	4,358	880	Formalin
				2,284	Formalin
				3,600	Formalin
2°S	1°57′S	139°45′W	4,293	3,593	Formalin
5°S	4°57′S	139°44′W	4,198	1,216	Formalin
				2,099	NaN_3
				2,209	Formalin
				2,316	$HgCl_2$
12°S	11°58′S	135°02′W	4,294	1,292	Formalin
				3,594	Formalin

Sample preservation and handling are as described by Honjo et al. (1995). Buffered formalin was generally used as a preservative and was placed in the trap cups prior to deployment. Formalin has previously been determined to be among the best choices for sample preservation in short-duration sediment trap deployments (Knauer et al. 1984), but formalin has not been extensively tested for use in longer duration moored trap experiments. In the EqPac program, a comparison of formalin, $HgCl_2$, and NaN_3 (as preservatives) was undertaken at the 5°S mooring site, and the N and carbon (C) stable isotopic results are discussed at the end of this section. After trap recovery, all samples were initially wet sieved and were then split by a McLane WSD-10 rotating wet-sediment splitter. The <1-mm fraction constituted the bulk of the sample mass, and all isotopic data are for this fraction alone. Large swimmers were also effectively excluded from this size fraction.

Samples of surface sediment fluff layers were obtained using a multicorer (Smith et al. 1996). This device gently lands on the seafloor prior to coring, such that there is minimal disturbance of the sediment–water interface. Upon retrieval, visible fluff layers were sampled using a syringe and were preserved for later analysis by freezing.

Isotopic analysis—NO_3^- was extracted from seawater for isotopic analysis using a Devarda's reduction to NH_3; this step was followed by diffusion onto acidified glass-fiber fil-

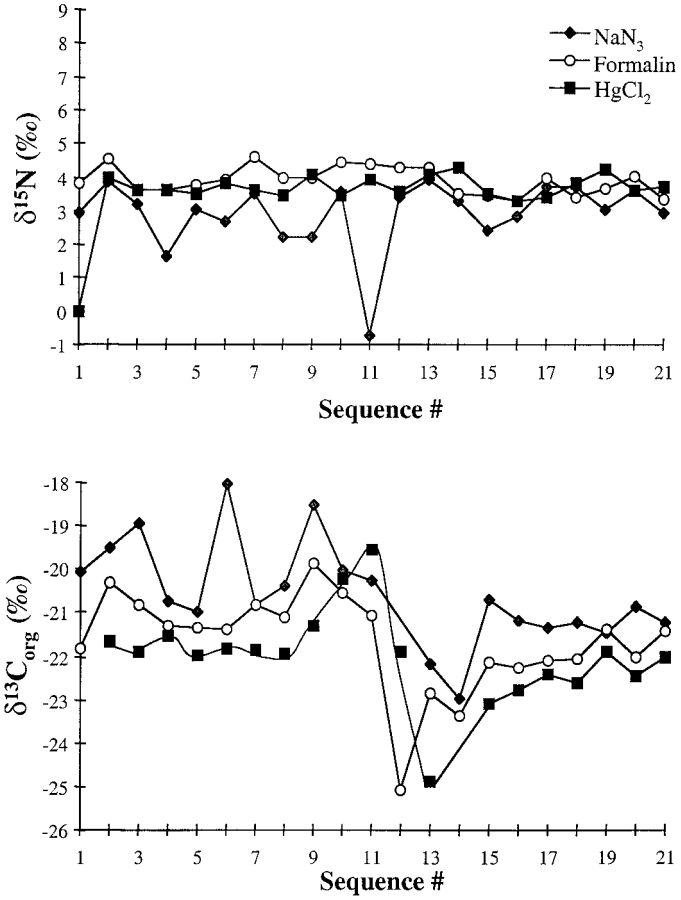

Fig. 1. Comparison of NaN_3, formalin, and $HgCl_2$ as trap preservatives at 5°S with respect to sediment trap $\delta^{15}N$ and $\delta^{13}C$ time-series data. Each preservative was placed in the cups of three separate sediment traps placed vertically within 100–200 m of each other on the trap mooring (*see* Table 1). Sequence No. refers to the trap cup number, and the time period of collection roughly corresponds to the date scales in Figs. 8–10. The $\delta^{15}N$ data for formalin preservation is the same as that found in Fig. 9 for the 5°S, 2,209-m trap.

ter through a Teflon membrane (Sigman et al. 1997). Recent improvements in this technique allow for near 100% yields and low blanks (<0.1 μmol), with reproducibility in $\delta^{15}N$ values for seawater samples equal to instrument performance.

Almost all N and organic C isotopic ratio measurements were made using an automated system consisting of an elemental analyzer coupled to a mass spectrometer for isotopic analyses in continuous flow mode (Owens and Rees 1989). Particulate matter samples were pretreated to remove inorganic C by fuming with concentrated HCl to facilitate measurement of $\delta^{13}C_{org}$. All samples were prepared for mass spectrometer analysis by encapsulation in tinfoil cups. Reproducibility for $\delta^{15}N$ and $\delta^{13}C$ was better than ± 0.2‰. Standardization is both by combustion of solid materials of known isotopic composition and by injections of standard gases into the carrier gas (helium). All $\delta^{15}N$ data are relative to atmospheric N_2, and $\delta^{13}C$ values are relative to the Pee Dee Belemnite (PDB) standard.

Sediment trap preservation experiment—At the 5°S site, the 2,209 m trap was loaded with formalin, whereas traps 200 m above and 100 m below employed NaN_3 and $HgCl_2$, respectively (Table 1). Specifics of the protocols and results for major elemental and mineralogical fractions are found in Honjo et al. (1995). $\delta^{15}N$ and $\delta^{13}C$ (organic) for the formalin and $HgCl_2$ traps are in excellent agreement, with no discernible change in their relationship with time (Fig. 1). The average difference is not significantly different from 0‰ for both of these parameters (Table 2). Average values for these properties as well as those for %N, %Corg (percent organic carbon), and C : N for the time series exhibit no descernable difference (Table 2). These results indicate that both preservatives are appropriate for $\delta^{15}N$ and organic $\delta^{13}C$ analysis. In particular, formalin does not appear to be adding sufficient organic C to the sample to alter $\delta^{13}C$. Use of NaN_3, though, produces larger and more erratic differences in isotopic composition and is clearly the less preferred choice for use. $\delta^{15}N$ values are clearly skewed lower, by about 1‰ on average (Table 2). This result may arise because the residual NaN_3 remains in the sample, although a concomitant increase in %N would have been expected.

Results and discussion

$\delta^{15}NO_3^-$ observations—Previously, the general inverse relationship between surface $[NO_3^-]$ and $\delta^{15}N$ of suspended and sinking POM was attributed to isotopic fractionation during NO_3^- uptake by phytoplankton. Compared to the lighter isotope of an element, slightly slower reaction rates are typically associated with the heavier isotope. Following this, phytoplankton preferentially incorporate $^{14}NO_3^-$ relative to $^{15}NO_3^-$ and have lowered $\delta^{15}N$ values when NO_3^- utilization is incomplete. By mass balance, $\delta^{15}NO_3^-$ also increases with its progressive drawdown. $\delta^{15}NO_3^-$ data from the S2 cruise (S2; August 1992; $\delta^{15}NO_3^-$ unavailable from S1) provide direct evidence for this effect. Observations include a vertical profile taken near the equator as well as underway samples taken across the surface $[NO_3^-]$ gradient (Figs. 2, 3A). As

Table 2. Comparison of results for the 5°S trap preservation experiment averaged over the deployment period. Standard deviations include the natural variability for the time series.

	$\delta^{15}N$ Avg. (SD)	$\delta^{13}C$ Avg. (SD)	C:N Avg. (SD)	%N Avg. (SD)	%C Avg. (SD)
NaN_3	2.9 (1.0)	−20.6 (1.2)	7.89 (0.46)	0.63 (0.09)	4.18 (0.53)
Formalin	3.9 (0.4)	−21.7 (1.1)	7.73 (0.33)	0.61 (0.09)	4.05 (0.66)
$HgCl_2$	3.7 (0.3)	−22.0 (1.1)	7.37 (0.69)	0.64 (0.12)	4.09 (0.64)

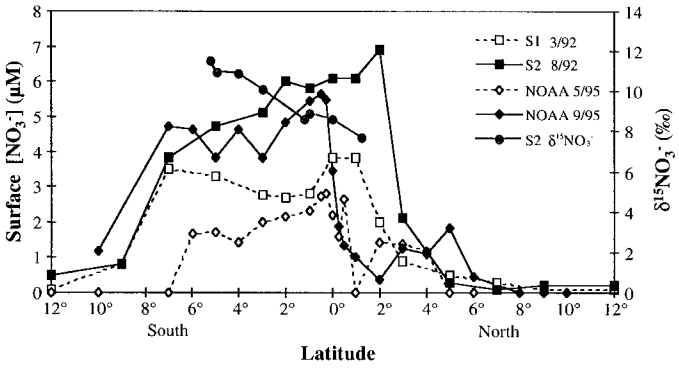

Fig. 2. Latitudinal distribution of near-surface $[NO_3^-]$ at different periods during the U.S. JGOFS EqPac program. There is a spring to fall doubling of surface $[NO_3^-]$ that corresponds to relaxation of El Niño conditions. $\delta^{15}NO_3^-$ data from S2 are shown for comparison and demonstrate the ^{15}N enrichment with decreasing $[NO_3^-]$. The S1 and S2 data are from the U.S. JGOFS database (http://www1.whoi.edu/jg/dir/jgofs/eqpac/). Data obtained by NOAA at additional time points are from their database (http://www.aoml.noaa.gov/ocd/oaces/eqpac92.html).

expected, $\delta^{15}NO_3^-$ increases with decreasing $[NO_3^-]$ in both instances. In the vertical profile, this effect is seen only within the euphotic zone, which is again consistent with its biological nature. An approximation to the Rayleigh fractionation equation can be used to estimate the fractionation factor in ‰ units (ϵ):

$$\delta^{15}NO_3^- = \delta^{15}NO_{3\,\text{initial}}^- - \epsilon \times \ln([NO_3^-]_{\text{obs.}}/[NO_3^-]_{\text{initial}}) \quad (1)$$

$\delta^{15}NO_{3\,\text{initial}}^-$ and $[NO_3^-]_{\text{initial}}$ refer to values prior to biological utilization. ϵ corresponds to $(R_{14}/R_{15} - 1) \times 1{,}000$, where R_{14}/R_{15} is the ratio of the specific reaction rates for ^{14}N and ^{15}N, respectively, In the literature, R_{14}/R_{15} is also referred to as a fractionation factor, α. The underway and profile data fall along the same regression line of $\delta^{15}NO_3^-$ and $\ln[NO_3^-]$ (Fig. 3B). A common value for ϵ is indicated by the strong linear relationship, estimated from the slope to be 5‰. This value is very similar to recent field observations that were also based on $\delta^{15}NO_3^-$ versus $\ln[NO_3^-]$ relationships (Table 3) in which improved methods for $\delta^{15}NO_3^-$ determination were employed (Sigman et al. 1997). In contrast, the estimates for ϵ, based on $\delta^{15}N$-PN data found in Table 3, have large uncertainties due to other factors that influenced the $\delta^{15}N$ of POM such as its trophic composition (Altabet 1996). We also consider the estimate for ϵ of 8–9‰ for the Subarctic Pacific (Altabet and Francois 1994*b*) to have been superseded by more recent studies because of the use of an inferior $\delta^{15}NO_3^-$ methodology. Taken together with this study's results, HNLC regions (Southern Ocean, Subarctic Pacific, and equatorial Pacific) all appear to have values for ϵ that are between 4 and 6‰. These regions vary greatly in average surface NO_3^- concentration, such that this parameter does not appear to influence ϵ. However, no reliable estimates of ϵ at very low $[NO_3^-]$ (e.g., <1 μM) have been made because of methodological limitations. By reducing the number of variable parameters, a near-constant value for ϵ facilitates practical application of $\delta^{15}N$ in paleoceanographic and modern marine biogeochemical studies. There may be a biological and ecological basis for this finding. The observed range in field estimates for ϵ is similar to some recent results for uptake of NO_3^- by diatoms in culture (e.g., Waser et al. 1998), and there is evidence that diatoms account for most of the NO_3^- uptake in HNLC regions (Landry et al. 1997).

Since the profile and underway data fall on a common $\delta^{15}NO_3^-$: $\ln[NO_3^-]$ relationship, a single initial $\delta^{15}NO_3^-$ and $[NO_3^-]$ for the region is implied. This observation is consistent with equatorial upwelling providing a common source

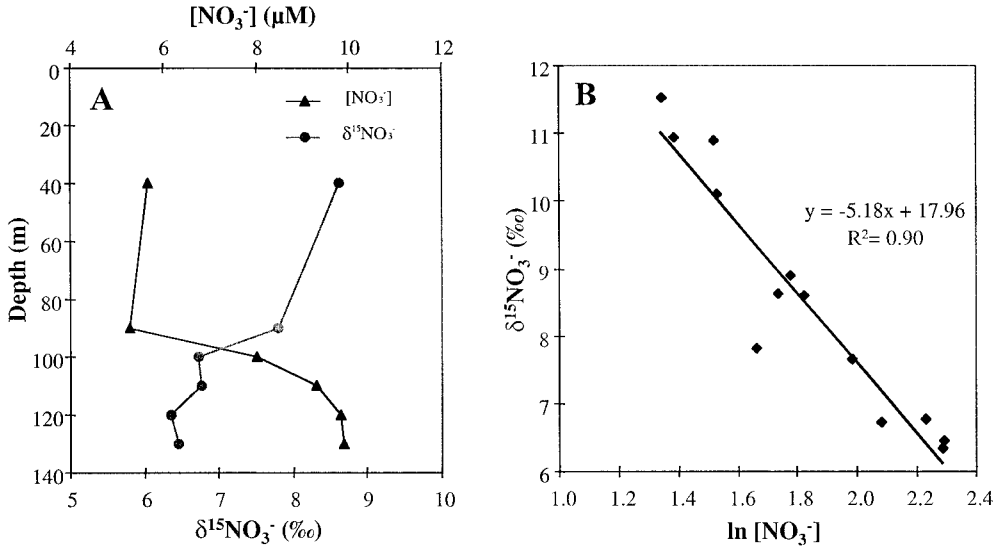

Fig. 3. (A) Vertical profile of $[NO_3^-]$ and $\delta^{15}NO_3^-$ at the equator during S2 showing relative ^{15}N enrichment with reduced $[NO_3^-]$ in the euphotic zone (ca. upper 100 m). (B) $\delta^{15}NO_3^-$ versus $\ln[NO_3^-]$ for this profile as well as near-surface data shown in Fig. 2. The linear trend is consistent with Rayleigh fractionation (*see* Eq. 1). The inverse slope of 5.2 estimates the fractionation factor (ϵ).

Table 3. Field estimates of the nitrogen isotope fractionation factor (ϵ) for nitrate uptake.

Region	Method	ϵ (‰)	Reference
Coastal			
Auke Bay, Alaska	δ^{15}N-PN vs $\delta^{15}NO_3^-$	4	Goering et al. 1990
Chesapeake Bay	δ^{15}N-PN vs $\delta^{15}NO_3^-$	7	Horrigan et al. 1990
Atlantic			
North Atlantic	δ^{15}N-PN vs $\delta^{15}NO_3^-$	8–9	Altabet et al. 1991
Pacific			
Western North Pacific	δ^{15}N-PN vs $[NO_3^-]$	5	Wada 1980
Subarctic Pacific	δ^{15}N-PN vs $\delta^{15}NO_3^-$	5–6	Wu et al. 1997
Western Subarctic Pacific	$\delta^{15}NO_3^-$ vs $[NO_3^-]$	9.1	Altabet and Francois 1994b
Monterey Bay	$\delta^{15}NO_3^-$ vs $[NO_3^-]$	5	Altabet et al. 1999
Southern Ocean			
Weddell Sea	δ^{15}N-PN vs $\delta^{15}NO_3^-$	8	Biggs et al. 1988
Antarctic Zone, east Indian	$\delta^{15}NO_3^-$ vs $[NO_3^-]$	5–6	Sigman et al. 1999
Antarctic Zone, central Pacific	$\delta^{15}NO_3^-$ vs $[NO_3^-]$	4–5	Sigman et al. 1999
Antarctic Zone, east Pacific	$\delta^{15}NO_3^-$ vs $[NO_3^-]$	4–5	Sigman et al. 1999
Subantarctic Zone, central Pacific	$\delta^{15}NO_3^-$ vs $[NO_3^-]$	4.5	Sigman et al. 1999

of NO_3^- to the system. Source $\delta^{15}NO_3^-$ is about 6.4‰, significantly higher than average marine $\delta^{15}NO_3^-$ (4.5–5.0‰; Sigman et al. 1997, 2000). Values of 6–7‰ are typical of upper thermocline waters in the eastern North Pacific as a result of denitrification in the east tropical North Pacific (Cline and Kaplan 1975). However, the source of NO_3^- to the equatorial Pacific is the equatorial undercurrent. This current is thought to originate to the west in the vicinity of New Guinea, with the New Guinea coastal undercurrent as its source (Tsuchiya et al. 1989; Toggweiler and Carson 1995). The elevated $\delta^{15}NO_3^-$ values for the undercurrent could result from recirculation of Pacific upper thermocline waters but may also have contributions from subantarctic mode water, which is also relatively ^{15}N enriched (Sigman et al. 1999).

Near-surface POM data—Near-surface, suspended POM for both the S1 and S2 cruises have δ^{15}N values that are, overall, inversely related to surface NO_3^- concentration (Fig. 4). Comparing the two observation periods, the δ^{15}N-POM values are remarkably similar as a function of latitude, despite the overall doubling of $[NO_3^-]$ between S1 and S2. δ^{15}N-POM ranges from 1‰ in the high-$[NO_3^-]$ zone to 17‰ at 12°S. These observations are qualitatively consistent with the latitudinal variations previously reported for annual average sediment trap δ^{15}N in this region (Altabet and Francois 1994*a*). An apparent departure from this general view is found during S2 (Fig. 4). The southward rise in $\delta^{15}NO_3^-$ (and decrease in $[NO_3^-]$, Fig. 2) between 1°N and 6°S co-occurs with relatively constant δ^{15}N-POM. Separation of scales of variability is likely responsible for this observation. δ^{15}N-POM responds to NO_3^- utilization integrated over the residence time for POM in the euphotic zone (Altabet and Francois 1994*b*). In contrast, $\delta^{15}NO_3^-$ can vary more rapidly with changes in physical supply and biological uptake.

Asymmetrical distributions in δ^{15}N-POM and $[NO_3^-]$ about the equator were observed during both cruises (Figs. 2, 4) and are found to correspond to the three-dimensional physical structure of the equatorial Pacific (Toggweiler and Carson 1995). Northward of 6°N in the westerly northern equatorial countercurrent, δ^{15}N-POM values decrease, probably as a result of the local NO_3^- supply dominating over horizontal advection from the equator. In contrast, the southern sector shows steadily rising δ^{15}N-POM with decreasing NO_3^-, indicating the importance of poleward advection as far south as 12°S. The S1 underway δ^{15}N-POM data are incomplete as a result of the failure of the uncontaminated seawater system. However, the S2 underway data clearly show with reasonable spatial resolution a smooth rise in δ^{15}N with latitude. At this distance from the equator, advection to the west from the southern equatorial current may bring residual surface NO_3^- from the Peruvian upwelling zone as well as from the eastern equatorial Pacific. Alternatively, subsurface NO_3^- originating in denitrifying regions off Peru and enriched in ^{15}N (Liu 1979) may be the cause of the high δ^{15}N-POM values. Denitrification-influenced NO_3^- can be advected far beyond its region of origin in suboxic intermediate waters (Liu and Kaplan 1989; Altabet et al. 1999). However, subeuphotic-zone $\delta^{15}NO_3^-$ at 12°S is about 7‰, close to values in the equatorial undercurrent (Fig. 3A) and up to 10‰ lower than the value for POM. At 12°S, NO_3^- is clearly delivered to the euphotic zone horizontally as a small residual of remote phytoplankton utilization.

Although the underway δ^{15}N-POM data provide very good spatial resolution, these 5-m samples (the depth of the ship's intake) may not well represent euphotic zone values if there is significant vertical variability. At major stations, euphotic zone averages from hydrocast samples for δ^{15}N-POM (upper 100 m) are compared to the underway data (Fig. 4). These hydrocast averages show the same general pattern in δ^{15}N about the equator as do the underway data. For S1, the hydrocast data show no particular trend with respect to the underway data, but for S2, they are typically lower by only about 1‰. S2 was characterized by a shallower thermocline and distinct δ^{15}N minima at the base of

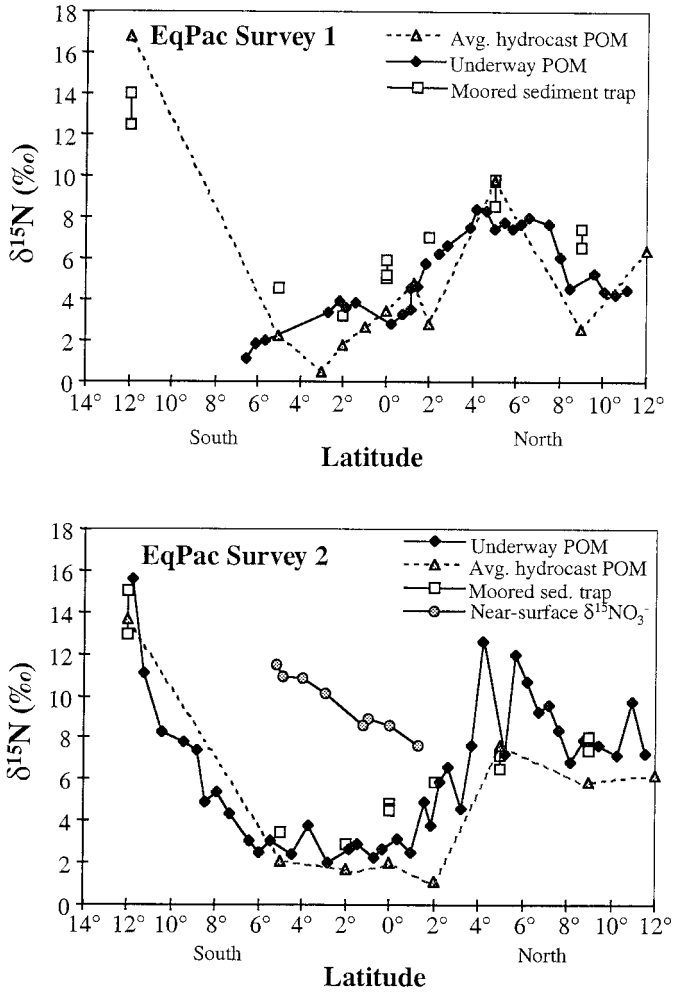

Fig. 4. Latitudinal distribution of $\delta^{15}N$ in near-surface, suspended particles (underway POM and hydrocast POM) and sinking particles collected by moored sediment trap for S1 (upper panel) and S2 (lower panel). The hydrocast POM $\delta^{15}N$ values are weighted averages for the upper 100 m. The moored sediment trap data are for samples corresponding to the 2-week period following station occupation during the S1 and S2 cruises, respectively. Trap depths at each site are listed in Table 1. For S2, the near-surface $\delta^{15}NO_3^-$ data are also presented.

the euphotic zone, which is the likely cause of this difference.

Comparison with sinking particles—Sinking particles collected by moored sediment traps at depths between 880 and 4,400 m (depending on site; Table 1) also show the same latitudinal distribution in $\delta^{15}N$. Here, values for samples synoptic with the S1 and S2 cruises, respectively (but delayed by 2 weeks to adjust for sinking speed), are shown (Fig. 4). Linear regressions between trap $\delta^{15}N$ and averaged hydrocast POM $\delta^{15}N$ have r^2 values of between 0.75 and 0.94 (Fig. 5). The slopes of about 1.2–1.3 are close to 1, indicating a constant offset in $\delta^{15}N$ between euphotic zone POM and moored trap POM. The 95% confidence intervals for the slopes of these regressions are ± 0.32 and 0.35, respectively, such that they are not significantly different from 1. The latitudinal variation in trap $\delta^{15}N$ evidently reflects the latitudinal variation in near-surface $\delta^{15}N$-POM. These results thus demonstrate tight coupling between euphotic zone processes and particle flux at depth. As previously observed (Altabet 1988), the negative intercepts show that sinking particles are, on average, several ‰ enriched in ^{15}N, as compared to near-surface POM. Although sinking POM $\delta^{15}N$ will reflect the average of new N uptake minus any fractionation, other factors can influence near-surface $\delta^{15}N$-POM. Of likely importance is phytoplankton utilization of recycled N, which was found to be important during EqPac (McCarthy et al. 1995). This source tends to be ^{15}N depleted (Altabet 1988; Checkley and Miller 1989), and its utilization would lower $\delta^{15}N$-POM values. The observations at 12°S are unusual in that moored traps have lower $\delta^{15}N$ than is found in the euphotic zone. Horizontal transport at depth of ^{15}N-depleted POM may be one explanation, since trap $\delta^{15}N$ decreases with depth (see below). Nevertheless, latitudinal changes in surface $\delta^{15}N$-POM predict well the relative variations in the $\delta^{15}N$ of sinking particles.

Comparisons of C : N ratios and $\delta^{13}C$ for underway POM and trap material show the two to be generally very similar in composition (Figs. 6, 7). Particularly for $\delta^{13}C$, the traps tend to track the slight latitudinal and temporal variation found in the near-surface POM. At the north and south extremes of the transects, trap $\delta^{13}C$ is lower than that for surface POM and is further evidence of possible horizontal sources of sinking particles. Overall, though, these results further demonstrate that isotopic gradients generated in surface waters are not obscured during the sinking of large particles through the water column by diagenesis or advection. By inference, this is likely also true for organic geochemical tracers.

S1/S2 comparison—Among a number of changes previously reported with relaxation of El Niño conditions, surface $[NO_3^-]$ doubled between S1 and S2 in the region between 4°S and 3°N (Fig. 2). Because of the dependence of $\delta^{15}N$ on nitrate drawdown, a significant decrease in $\delta^{15}N$ for NO_3^-, near-surface POM, and sediment trap samples would be expected for S2, on the order of 4‰ (*see* Eq. 1). In fact, a change in $\delta^{15}N$ is either nil or opposite in sign to expectations, as observed in suspended and sinking POM (Fig. 4). $\delta^{15}N$, whether in NO_3^- or POM, does not respond directly to variations in NO_3^- concentration but responds instead to its fractional utilization (Altabet 1996). Curiously, these results indicate little change in the fractional utilization of NO_3^- (u) between cruises S1 and S2.

$$u = NO_3^- \text{ utilization}/NO_3^- \text{ supply} \quad (2)$$

$$u = 1 - f \quad (3)$$

Constant u with increase in $[NO_3^-]$ would imply a proportional increase in total NO_3^- utilization by phytoplankton, with increases in equatorial upwelling flux of NO_3^-. Between S1 and S2, physical, chemical, and biological data show that upwelling, primary production, and NO_3^- uptake all increased by approximately a factor of 2 (McCarthy et al. 1995; Landry et al. 1997). The $\delta^{15}N$ data can be used to calculate u. Using Eq. 1 with $\epsilon = 5‰$, $\delta^{15}NO_{3\ \text{initial}}^- = 6.4‰$,

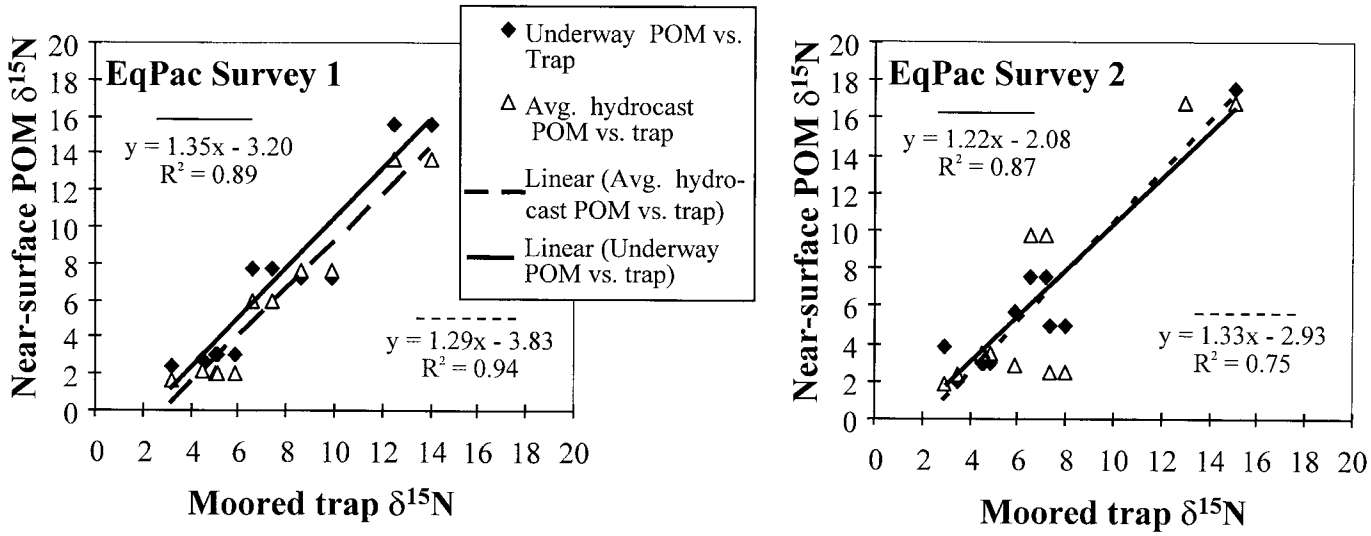

Fig. 5. Near-surface POM δ^{15}N versus moored trap δ^{15}N for S1 (right panel) and S2 (left panel). As in Fig. 4, the moored sediment trap data are for samples corresponding to the 2-week period following station occupation during the S1 and S2 cruises, respectively. The hydrocast POM δ^{15}N values are weighted averages for the upper 100 m. The underway POM δ^{15}N data used in this plot are only for samples collected at the corresponding trap sites. The separate but similar regressions with moored trap δ^{15}N for underway and hydrocast POM indicate tight coupling between surface processes and the isotopic composition of deeply sinking particles. The negative intercept is the likely result of trophic transfers (*see text*).

and a euphotic zone $\delta^{15}NO_3^-$ value of 8.6‰ (measured at 0° during S2), u is near 0.4 (60% unutilized). An independent calculation can be made using the sediment trap data and the instantaneous form of the Rayleigh fractionation equation, as follows:

$$\delta^{15}N_{trap} = \delta^{15}NO_{3\ initial}^- - \epsilon \times \ln(1 - u) - \epsilon \quad (4)$$

Using Eq. 4 and average sediment trap values for S2 (4.6‰), a similar value for u is derived (0.5 or 50% utilization). During S1 ($\delta^{15}N_{trap}$ = 5.4‰), a value for u of 0.55 (45% unutilized) is calculated, demonstrating the small change in relative utilization between the two periods.

The above calculations use the instantaneous form of the Rayleigh fractionation equation. With respect to integrated properties, the system may be viewed as being ''open,'' with continual supply of NO_3^- along with removal of organic N. In this respect, equations appropriate for chemostats may be used for comparison (Barford et al. 1999).

$$\delta^{15}NO_{3\ avg.euphotic\ zone}^- = \delta^{15}NO_{3\ initial}^- + \epsilon \times (1 - u) \quad (5)$$

Expected values for sinking particles may be calculated by mass balance:

$$\delta^{15}N_{trap} = [(\delta^{15}NO_{3\ initial}^- - \delta^{15}NO_{3\ avg.euphotic\ zone}^-) \times (1 - u)]/u \quad (6)$$

Using Eq. 5, for S2, a slightly higher value of u is calculated (0.56). The expected value for sinking particles from Eq. 6 exactly matches observations (4.6‰). Regardless of the specific equations used, the conclusion remains that the small changes in δ^{15}N between S1 and S2 demonstrate similar fractional utilization of NO_3^- near 0.5. If u is similar but $[NO_3^-]$ has doubled, there must have been coordinated increases in both the upwelling and biological uptake of NO_3^-. Such correlation indicates that there is a specific mechanism controlling u, such as Fe limitation of NO_3^- uptake.

Time-series sediment trap results—The near-surface POM and moored sediment trap δ^{15}N signals are tightly coupled during both S1 and S2. Consequently, the sediment trap time series should provide a more highly temporally resolved record of δ^{15}N variations during the entire JGOFS EqPac program. This is particularly important during the transition from El Niño to more normal conditions when no other observations are available. Starting at the equator (Fig. 8), δ^{15}N falls within a relatively narrow range of 4–6‰ for the entire sampling period. In contrast to some prior studies, there is no significant change in δ^{15}N for sinking particles with depth. In the North Atlantic, for example, trap δ^{15}N was observed to decrease with depth during periods of very low particle flux (Altabet et al. 1991). Evidently, particle flux at the equator is sufficiently high at all times, such that flux from the surface overwhelms any horizontal transports/sources in the ocean's interior or other modifying factors. Trap δ^{15}N values were found to be highest in April 1992 after the S1 observations, with modestly decreasing values through the transition from El Niño to more normal conditions. Nutrient data from NOAA's RV *Baldridge* show surface $[NO_3^-]$ during the peak in δ^{15}N to be even lower than during S1. The trap time series at the equator confirms the view of little change in relative nutrient utilization during the EqPac program, with a range in u of 0.4 to 0.6.

Relative to trap δ^{15}N, PN flux is more variable at the equator (Fig. 8), the 880-m trap in particular showing strong spikes in flux that are associated with the passage of instability waves (Honjo et al. 1995). Whereas δ^{15}N is an intrinsic property, PN flux is an extrinsic one. Changes in the dispersion of sinking particles by horizontal advection or var-

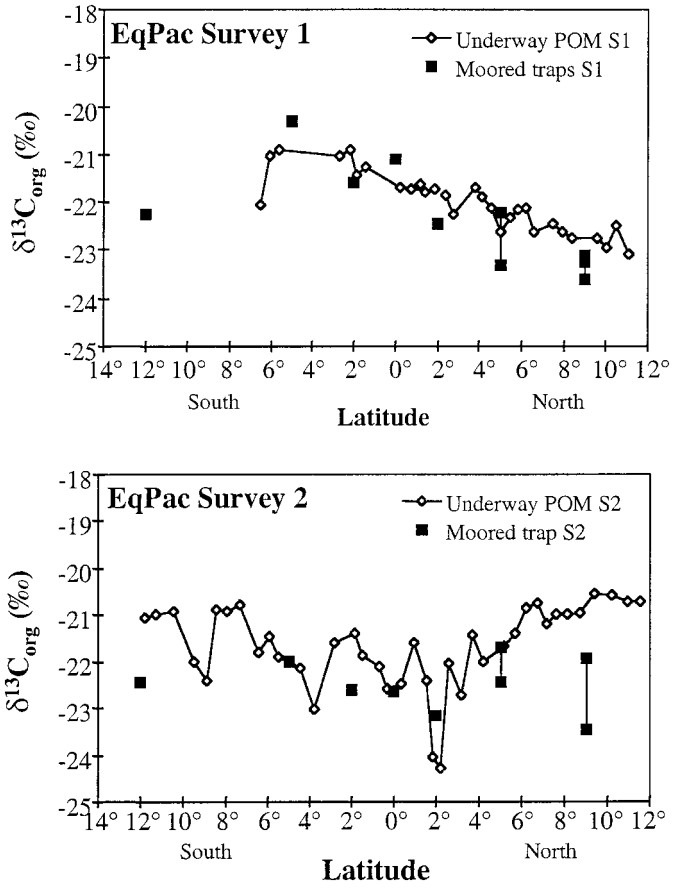

Fig. 6. Latitudinal distribution of underway POM and moored sediment trap $\delta^{13}C$ for S1 (upper panel) and S2 (lower panel). The moored sediment trap data are for samples corresponding to the 2-week period following the date of underway sampling at each trap site.

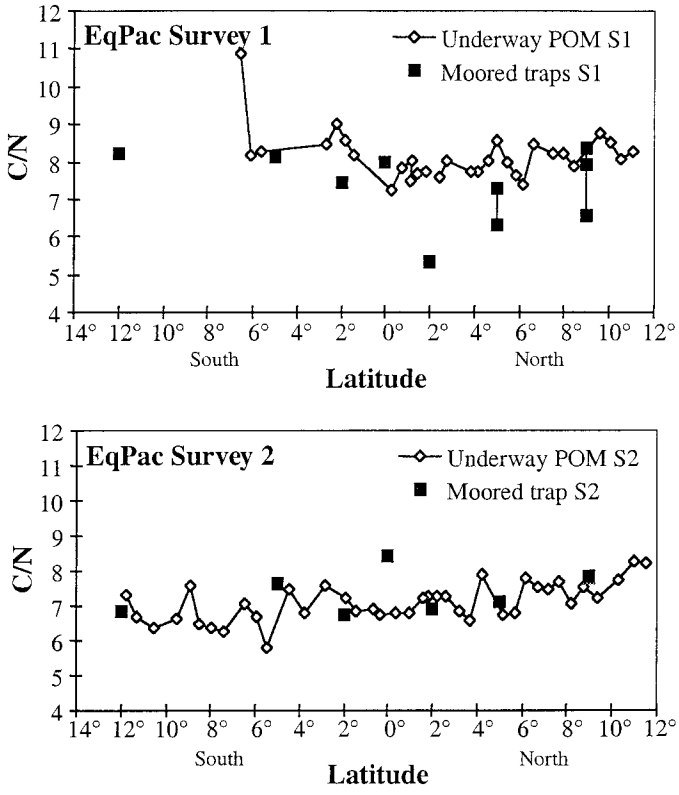

Fig. 7. Latitudinal distribution of underway POM and moored sediment trap C : N ratios for S1 (upper panel) and S2 (lower panel). The moored sediment trap data are for samples corresponding to the 2-week period following the date of underway sampling at each trap site.

iations in trapping efficiency would alter PN flux but not necessarily trap $\delta^{15}N$. The 3,600-m trap results indicate a weak relationship between PN flux and $\delta^{15}N$. In the first half of the observation period, PN fluxes rose and fell with trap $\delta^{15}N$, and increasing PN flux might have been partially coupled with small increases in relative nutrient utilization. In the second half of the observation period, though, the smaller maximum in PN flux appeared to be unrelated to trap $\delta^{15}N$.

At 2°S and 5°S (Fig. 9), the temporal range in trap $\delta^{15}N$ is only 1–1.5‰. Similar to the equator data, values tend to be higher in the middle third of the time series and lowest in the last third of the time series, although these variations are slight compared to those noted north of the equator. PN flux at 2°S and 5°S is punctuated by a large peak in August 1992; this peak is likely associated with instability waves. At 12° S, trap $\delta^{15}N$ is substantially increased by about 10‰ relative to the equator, as noted before (Fig. 4). A small decrease in trap $\delta^{15}N$ with depth is apparent for part of the time series. This site has very low particle flux, and horizontal transport at depth of material relatively depleted in ^{15}N may be an explanation. The range in trap $\delta^{15}N$ for the time series is still modest (3‰) but is greater than the variations at 0°, 2°S, and 5°S. Overall, the dominant changes in $\delta^{15}N$ south of the equator are latitudinal and not temporal in nature. The latitudinal gradient in nutrient utilization measured by trap $\delta^{15}N$ is a consistent feature of this part of the system. However, small perturbations are apparent. Two trap $\delta^{15}N$ peaks of about 1–2‰ in amplitude occurred simultaneously in February and May 1992 at 0°, 2°S, 5°S, and 12°S. At 12°S, these events are clearly associated with maxima in PN flux. At 2°S and 5°S, the association is weaker. A simple explanation would be that widespread increased nutrient utilization produced increased new production. Forcing through changes in equatorial upwelling rate or chemistry of upwelled waters, though, is inconsistent with the simultaneous nature of the events.

Going north of the equator and to lower surface $[NO_3^-]$, there is progressively higher sediment trap $\delta^{15}N$ at the 2°N and 5°N sites (Fig. 10). The time series themselves are distinguished by a large 5‰ amplitude of temporal variation. At both sites, significant decreases in trap $\delta^{15}N$ between July and October 1992 also occurred during the transition period from ENSO to more normal conditions. The increase in surface $[NO_3^-]$ accompanying this transition was the result of a net northward movement of a surface NO_3^- front in this latitude band (Fig. 2). The 2°N and 5°N sediment trap $\delta^{15}N$ data are best explained by the northward movement of waters that had experienced less NO_3^- depletion during the re-

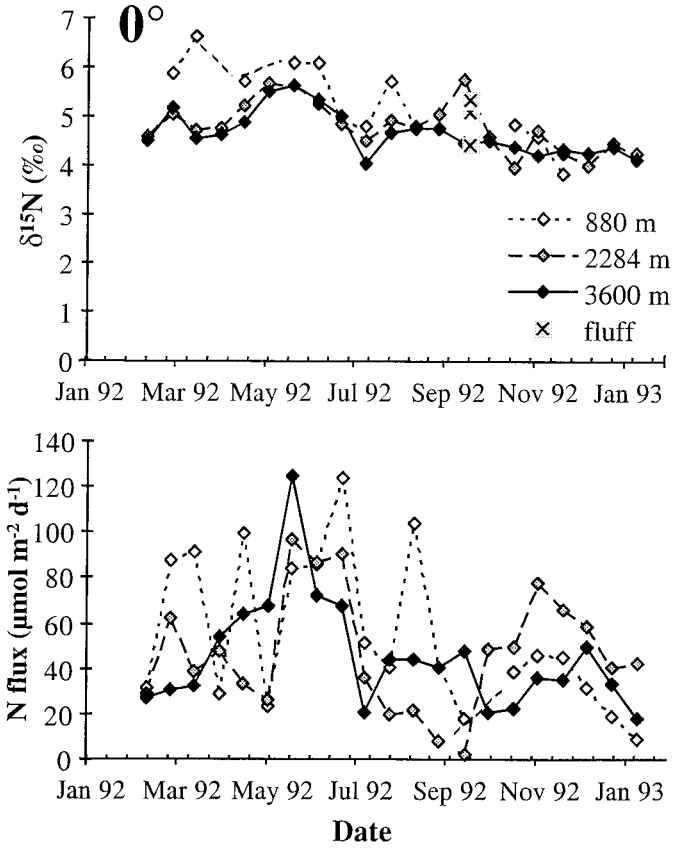

Fig. 8. Sediment trap time-series data at the equator for δ^{15}N (upper panel) and particulate N flux (lower panel). Seafloor fluff δ^{15}N is plotted at the time of its collection. Although there is substantial temporal variability in N flux, there is relatively little change in δ^{15}N with either depth or time. Additionally, the fluff δ^{15}N is indistinguishable from co-occurring trap δ^{15}N.

turn from El Niño to more normal conditions. The surface nutrient data do not have sufficient temporal resolution to provide a detailed view of the transition from El Niño, and the data sets available are likely influenced by mesoscale variability in the form of instability waves. The sediment trap data, in contrast, are highly temporally resolved, and the 2°N data show the major transition occurring between July and October 1992. At 5°N, the onset of the transition is a month later. Because of differences with depth, the end of the transition is not clear, occurring in October–November 1992. These data can be interpreted as an increasing northward expression of the northern equatorial current occurring over a 4-month period with, at most, a 1-month delay between 2°N and 5°N.

The temporal change in δ^{15}N in this latitude zone can be used as a ''natural'' tracer experiment to test the dynamic linkages between biogeochemical reservoirs and fluxes on a large scale (Altabet 1996). This approach is well suited for assessing the relative age of seafloor ''fluff'' layers collected during the U.S. JGOFS EqPac benthic cruise (TT013). Chemical and microscopic analysis indicates that this material is mostly relatively ''fresh'' phytodetritus (Smith et al. 1996). Along with the sediment trap time series, δ^{15}N values for fluff material are plotted at the time point corresponding to their date of collection. Coeval fluff and sediment trap δ^{15}N values are indistinguishable at 0°, 2°N, and 5°N (Figs. 8, 10). The fluff δ^{15}N values plot exactly with the sediment trap values despite the temporal decrease in trap δ^{15}N observed prior to their collection. These results are in contrast to the 4‰-higher values for the consolidated sediment layer immediately below (Altabet and Francois 1994*a*,*b*). The δ^{15}N results indicated that fluff material at these sites was recently deposited and was not likely to be more than 1 month old. Radioisotope study results are consistent with these findings (Smith et al. 1996). Diagenetic alteration of δ^{15}N would increase δ^{15}N values and thus make the fluff material appear

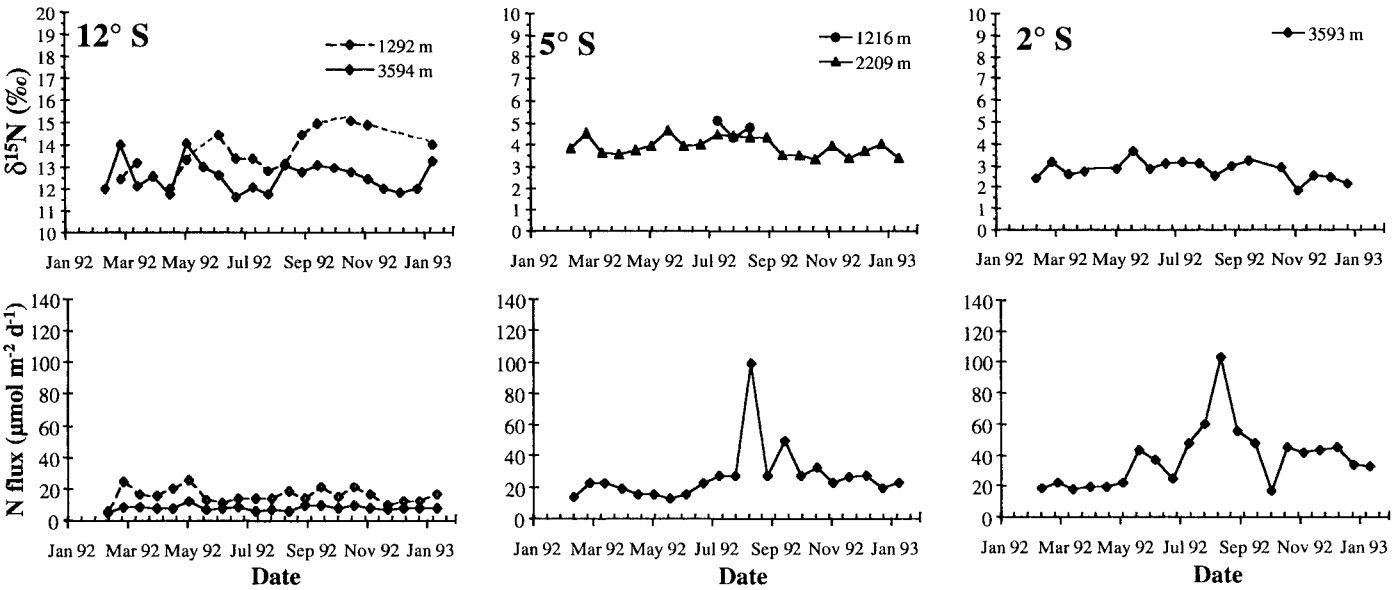

Fig. 9. Sediment trap time-series data at 2°S, 5°S, and 12°S for δ^{15}N (upper panel) and particulate N flux (lower panel). Note change in δ^{15}N scale for 12°S. Although there is little temporal variation in δ^{15}N, there is substantial southward increase.

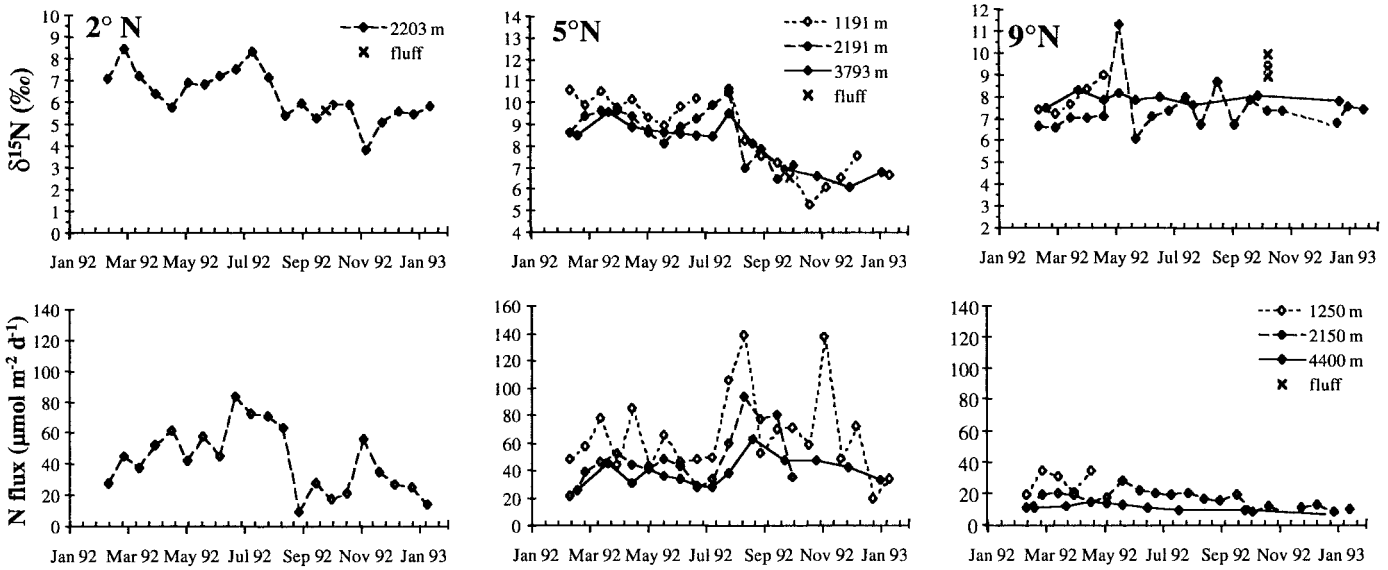

Fig. 10. Sediment trap time-series data at 2°N, 5°N, and 9°N for $\delta^{15}N$ (upper panel) and particulate N flux (lower panel). Note the changes in vertical scale. The 2°N and 5°N $\delta^{15}N$ time series exhibit significant decreases in $\delta^{15}N$ during the relaxation of El Niño conditions. Seafloor fluff $\delta^{15}N$ is plotted at the time of its collection. Except at 9°N, the fluff $\delta^{15}N$ is indistinguishable from co-occurring trap $\delta^{15}N$.

to be older. If fluff material had a relatively long lifetime on the seafloor, $\delta^{15}N$ would also be higher, reflecting an averaging of sediment trap values over the prior several months or more. Thus, the $\delta^{15}N$ results also imply rapid turnover of the fluff material between 0° and 5°N, probably through consumption by benthic animals (Smith et al. 1996).

Relative to the sites immediately to the south, the region north of 9°N had lower values for the $\delta^{15}N$ of surface water POM during both S1 and S2 (Fig. 4). It follows that this latitude band has substantially reduced influence from the equatorial zone, and local sources of new N would be more important than ^{15}N-enriched NO_3^- advected from the equator. Correspondingly, the 9°N sediment trap $\delta^{15}N$ data do not exhibit the strong temporal variations observed at 2°N and 5°N, which are associated with relaxation of El Niño. In contrast to the sites to the south, seafloor fluff samples have $\delta^{15}N$ values that are about 2‰ enriched relative to those of the sediment traps. It appears that this material has undergone some degree of degradation and is less ''fresh.''

Control of fractional nutrient utilization—It has been noted that despite a doubling of surface $[NO_3^-]$ concentrations during the observation period, $\delta^{15}N$ values varied only modestly. This is seen for both the S1 and S2 surface POM data and for the more highly temporally resolved sediment trap data. The region between 2°N to 5°N is an exception; in this region, decreases in $\delta^{15}N$ over the observation period are associated with northward expansion of surface waters with elevated macronutrient content. Near constancy in $\delta^{15}N$ values at the equator implies near constancy in fractional NO_3^- utilization and thus a simultaneous increase in both the upwelled flux of NO_3^- and in its utilization:

$$U_{NO_3^-} = W \times [NO_3^-]_{upwelled} - A \times [NO_3^-]_{surface} \quad (7)$$

In this equation, U is NO_3^- uptake, W is the upwelling rate, and A is net horizontal advection of the surface layer away from the upwelling zone. Since net horizontal advection at the surface must equal upwelling at the equator,

$$U_{NO_3^-} = W \times ([NO_3^-]_{upwelled} - [NO_3^-]_{surface}) \quad (8)$$

and rearranging:

$$U_{NO_3^-}/W = [NO_3^-]_{upwelled} - [NO_3^-]_{surface}, \quad (9)$$

dividing both sides by $[NO_3^-]_{upwelled}$:

$$U_{NO_3^-}/(W \times [NO_3^-]_{upwelled}) = 1 - [NO_3^-]_{surface}/[NO_3^-]_{upwelled} = u \quad (10)$$

The left-hand side of the equation is the same as the fractional utilization term (u) in Eq. 3. U and $W \times [NO_3^-]_{upwelled}$ must change proportionally when u remains constant.

A controlling mechanism such as Fe limitation of NO_3^- drawdown must keep u within a narrow range despite large changes in upwelling rate, productivity, etc. In the equatorial Pacific, Fe availability has been shown to be a limiting factor for phytoplankton growth and a regulator of macronutrient utilization (Landry et al. 1997). In most regions of the open ocean, Fe is supplied primarily by aeolian transport (Duce 1986; Duce and Tindale 1991; Johnson et al. 1997), such that its flux to the surface ocean is decoupled from the flux of NO_3^-. However, in the equatorial Pacific, Fe is thought to be supplied primarily by upwelling (Gordon et al. 1997), and, consequently, its flux is directly linked to the flux of macronutrients by vertical advection. This linkage likely produces the mechanism by which relatively constant u is maintained.

Assuming that biologically available Fe is supplied only by upwelling and is completely utilized in the euphotic zone, relative NO_3^- utilization should be a function of the product of Fe/NO_3^- in upwelled waters and the average phytoplankton NO_3^- : Fe utilization ratio. Since Fe is limiting, its uptake will equal the supply from upwelling:

$$U_{Fe} = [Fe]_{upwelled} \times W \quad (11)$$

The uptake of other nutrients will then be controlled by their ratios of utilization with Fe.

$$U_{NO_3^-} = U_{Fe} \times \{NO_3^-/Fe\}_{util.}$$
$$= [Fe]_{upwelled} \times W \times \{NO_3^-/Fe\}_{util.} \quad (12)$$

By substituting into Eq. 9 and eliminating common terms,

$$u = [Fe]_{upwelled}/[NO_3^-]_{upwelled} \times \{NO_3^-/Fe\}_{util} \quad (13)$$

Note that upwelling rate, and thus the upwelling flux of Fe or NO_3^-, does not have a direct influence on u. This derivation is consistent with our observations.

The upwelled Fe : NO_3^- ratio is likely an intrinsic property of the source of upwelled water in the equatorial undercurrent. The limited available data indicate a ratio of 12.2 ± 3.3 μmol mol^{-1} for the 100–200-m depth interval at the equator (data from Coale et al. 1996). Using Eq. 12 and a value for u of 0.5, a N : Fe uptake ratio of 0.04 mol μmol^{-1} is indicated. This result compares well with minimum N : Fe uptake ratios for Fe-limited phytoplankton in culture, 0.01–0.06 mol μmol^{-1}, indicated by cellular C : Fe data (Sunda and Huntsman 1995). Given that the [Fe] : [NO_3^-] ratio in upwelled waters is fixed by the chemistry of their sources, little change in observed u indicates that the NO_3^- : Fe utilization ratio was also relatively fixed during the observation period. The conclusion reached is that under these conditions, the relative utilization of upwelled NO_3^- is controlled to a near-constant value by the product of the Fe : NO_3^- ratio delivery by upwelling and NO_3^- : Fe utilization. In effect, the δ^{15}N of NO_3^- and suspended and sinking POM at the equator measures the limitation of NO_3^- utilization by Fe availability.

Of course, poleward from the equator there is additional NO_3^- utilization without additional upwelling of Fe. This NO_3^- drawdown is likely fueled by aeolian supply of Fe or by more efficient recycling of Fe, relative to N, in the euphotic zone. However, the control of new production by upwelled Fe is underscored when we consider that about 50% of NO_3^- drawdown occurs in the immediate vicinity of the equator. The balance is consumed over the much larger area between approximately 10°S and 6°N at 140°W.

Si limitation of diatom growth has also been hypothesized to regulate NO_3^- drawdown and new production in the equatorial Pacific (Dugdale and Wilkerson 1998). The equatorial undercurrent does appear to have silicate : NO_3^- ratios (of about 0.8; JGOFS database), less than preferred by diatoms. However, during S1 and S2, surface silicate concentrations at the equator were between 2.0 and 2.5 μM, despite the doubling in [NO_3^-]. Although there is a recognition that Si has a role in regulating new production, which varies with Fe limitation (Hutchins and Bruland 1998; Takeda 1998), it appears that in the vicinity of the equator, Si availability is not controlling u.

Paleoceanographic implications—Despite diagenetic increases, downcore sediment δ^{15}N should record past changes in the δ^{15}N of particles sinking to the seafloor (Altabet and Francois 1994*a*) and, thus, past changes in the δ^{15}N of near-surface POM and NO_3^-. Farrell et al. (1995) have shown an increase in δ^{15}N of 2.5–4‰ at the last glacial termination in near-equatorial cores well to the east of the JGOFS study region. Their interpretation called for decreased upwelling during this climate transition that reduced both productivity and surface [NO_3^-]. Sediment δ^{15}N for PC72 (0°, 140°W) collected during the JGOFS program is presented in Fig. 11. The data series spans the last 600 kyr, a period that is equivalent to about six glacial cycles. Repeated increases in δ^{15}N of about 1.5–2‰ occur at glacial terminations. This amplitude is smaller than that observed by Farrell et al. (1995), perhaps because of the westward location of the EqPac study region. The long-term downward trend is likely diagenetic in nature (Altabet in prep.) Spectral analysis shows peaks in spectral power at the orbital periodicities of 100 and 23 kyr. A 40-kyr periodicity is not apparent. The benthic δ^{18}O record (Fig. 11) is coherent at these periods, with no significant phase lag.

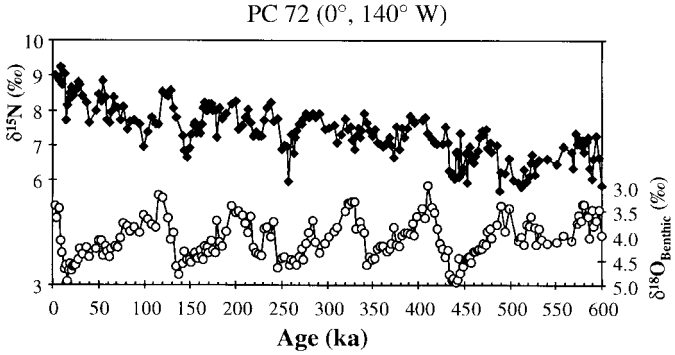

Fig. 11. A paleoceanographic record for δ^{15}N at the equator for the last 600 kyr. The bulk sediment δ^{15}N and benthic foraminiferal δ^{18}O are from piston core PC 72, collected during the benthic cruise of the U.S. JGOFS EqPac Program. Age model and δ^{18}O data were provided by A. Mix (OSU). δ^{15}N shows modest cyclicity correlated with glacial cycles, as illustrated by the δ^{18}O data. The long-term decrease in δ^{15}N is likely diagenetic in nature.

Based on our water column and sediment trap results, δ^{15}N records cannot be directly interpreted in terms of changing surface [NO_3^-] or export productivity but only in terms of relative nutrient utilization (assuming constant source $\delta^{15}NO_3^-$). In the Southern Ocean we have shown glacial increases in δ^{15}N (higher u) that are concurrent with reduced export productivity (Francois et al. 1997). It was concluded that the physical supply of NO_3^- to the euphotic zone via vertical transport had to be sharply reduced. Similarly, both the PC72 results and the results of Farrell et al. (1995) should be interpreted in terms of reduced glacial NO_3^- utilization, assuming little change in $\delta^{15}NO_{3\,initial}^-$. Our data and the analysis above further indicate that changes in upwelling and productivity, per se, were not the direct cause. Instead, there was a glacial increase in relative limitation by Fe. Either changes in the upwelled ratio of Fe and NO_3^- or changes in their utilization ratio occurred. The former is certainly possible. The origin of the equatorial undercurrent is off the coast of eastern New Guinea (Tsuchiya et al. 1989; Butt and Lindsrom 1994), and its Fe content is likely derived from exposure to the region's continental shelf and slope (Wells et al. 1999). Wells et al. (1999) further argued that tectonic processes in this vicinity over the last 10 million years would

have altered the Fe content of the equatorial undercurrent. High accumulation of fossil diatoms in late Miocene sediments from the eastern equatorial Pacific correlated with a period of suspected higher Fe. Though not necessarily as dramatic an effect, lower glacial sea level may have also affected the Fe content of the undercurrent and upwelled waters along the equator through reduction in continental shelf area. Relative nutrient utilization would decrease, as recorded by the downcore $\delta^{15}N$ data.

Conclusions

Changes in the relative utilization of NO_3^- in surface waters drive the large-scale variations in $\delta^{15}N$ observed in the equatorial Pacific. These isotopic signals are observed in dissolved NO_3^-, surface POM, deeply sinking particles, as well as in seafloor fluff. From our limited $\delta^{15}NO_3^-$ data, the fractionation factor for NO_3^- uptake is about 5‰, similar to that recorded during observations in other oceanic settings and consistent with NO_3^- uptake by diatoms. Whether as a vertical profile at the equator or as a surface transect, the $\delta^{15}NO_3^-$ data fell within the same Rayleigh fractionation relationship. There was a twofold increase in surface $[NO_3^-]$ between the S1 and S2 cruises, which corresponded to a relaxation of El Niño conditions. Nevertheless, the near-surface $\delta^{15}N$ POM data are very similar between these observation periods. The sediment trap time series provide a more highly resolved temporal record for changes in $\delta^{15}N$ over this period. At the equator and to the south, there is little variation, despite large changes in particle flux. An exception is in the 2°–5° N region, where there is substantial reduction in $\delta^{15}N$ with the relaxation of El Niño. Here there is a clear northward movement of NO_3^--rich water, a likely result of strengthening of the northern equatorial current. These temporal variations in $\delta^{15}N$ can be used as natural tracer experiments, and here fluff material is shown to have only recently arrived on the seafloor at 2°N and 5°N.

The near-constant relative utilization of NO_3^- at the equator despite a doubling in upwelling and surface $[NO_3^-]$ implies a controlling mechanism. Fe is a likely candidate, since it has been shown to be the limiting factor in this region and is supplied chiefly by upwelling. Theoretically, u is set by the product of the $Fe:NO_3^-$ supply ratio in upwelled waters and the phytoplankton NO_3^-he $Fe:NO_3^-$ supply is fixed by the chemistry of source waters, whereas $NO_3^-:Fe$ uptake should be a product of the phytoplankton species present. Since these ratios may be conserved parameters of the modern system, the observed narrow variations in u are sensible. The observed values of u of near 0.5 are consistent with given available data for the $Fe:NO_3^-$ supply ratio and the $NO_3^-:Fe$ uptake ratio. Since $\delta^{15}N$ values reflect u, they can thus be used to measure what is effectively the relative limitation of NO_3^- drawdown by Fe availability. Past variations in $\delta^{15}N$ from equatorial Pacific sediment cores need to be interpreted in this light. Glacial lowering of $\delta^{15}N$ is consistent with reduced $Fe:NO_3^-$ ratios in upwelled waters (greater Fe limitation) as a possible consequence of lower sea level influencing the Fe content of the equatorial undercurrent.

References

ALTABET, M. A. 1988. Variations in nitrogen isotopic composition between sinking and suspended particles: Implications for nitrogen cycling and particle transformation in the open ocean. Deep-Sea Res. **35:** 535–554.

———. 1989. A time-series study of the vertical structure of nitrogen and particle dynamics in the Sargasso Sea. Limnol. Oceanogr. **24:** 1185–1201.

———. 1996. Nitrogen and carbon isotopic tracers of the source and transformation of particles in the deep sea, p. 155–184. *In* V. Ittekkot, P. Schäfer, S. Honjo, and P. J. Depetris [eds.], Particle flux in the ocean. Wiley.

———, AND W. G. DEUSER. 1985. Seasonal variations in natural abundance of ^{15}N in particles sinking to the deep Sargasso Sea. Nature **315:** 218–219.

———, W. G. DEUSER, S. HONJO, AND S. STIENEN. 1991. Seasonal and depth-related changes in the source of sinking particles in the N. Atlantic. Nature **354:** 136–139.

———, AND R. FRANCOIS. 1994*a*. Sedimentary nitrogen isotopic ratio as a recorder for surface ocean nitrate utilization. Global Biogeochem. Cycles **8:** 103–116.

———, AND ———. 1994*b*. The use of nitrogen isotopic ratio for reconstruction of past changes in surface ocean nutrient utilization, p. 281–306. *In* R. Zahn, M. Kaminski, L. Labeyrie, and T. F. Pederson [eds.], Carbon cycling in the glacial ocean: Constraints on the ocean's role in global change. Springer-Verlag.

———, C. PILSKALN, R. THUNELL, C. PRIDE, D. SIGMAN, F. CHAVEZ, AND R. FRANCOIS. 1999. The nitrogen isotope biogeochemistry of sinking particles from the margin of the eastern North Pacific. Deep-Sea Res. **46:** 655–679.

BARFORD, C. C., J. P. MONTOYA, M. A. ALTABET, AND R. MITCHELL. 1999. Steady-state nitrogen isotope effects of N_2 and N_2O production in *Paracoccus* denitrificans. Appl. Environ. Microbiol. **65:** 989–994.

BUTT, J., AND E. LINDSROM. 1994. Currents off the east coast of New Ireland, Papua New Guinea, and the relevance to regional undercurrents in the western equatorial Pacific Ocean. J. Geophys. Res. **99:** 12503–12514.

CHAI, F., S. T. LINDLEY, AND R. T. BARBER. 1996. Origin and maintenance of high nitrate condition in the equatorial pacific. Deep-Sea Res. **43:** 1031–1064.

CHAVEZ, F. P., AND R. T. BARBER. 1987. An estimate of new production in the equatorial Pacific. Deep-Sea Res. **34:** 1229–1243.

CHECKLEY, D. M., JR., AND C. A. MILLER. 1989. Nitrogen isotope fractionation by oceanic zooplankton. Deep-Sea Res. **36:** 1449–1456.

CLINE, J. D., AND I. R. KAPLAN. 1975. Isotopic fractionation of dissolved nitrate during denitrification in the eastern tropical North Pacific Ocean. Mar. Chem. **3:** 271–299.

COALE, K. H., S. E. FITZWATER, R. M. GORDON, K. S. JOHNSON, AND R. T. BARBER. 1996. Control of community growth and export production by upwelled iron in the equatorial Pacific Ocean. Nature **379:** 621–624.

DUCE, R. A. 1986. The impact of atmospheric nitrogen, phosphorous, and iron species on marine biological productivity, p. 497–529. *In* P. Buat-Ménard [ed.], The role of air–sea exchange in geochemical cycling. Reidal.

———, AND N. W. TINDALE. 1991. Atmospheric transport of iron and its deposition in the ocean. Limnol. Oceanogr. **36:** 1715–1726.

DUGDALE, R. C., AND F. P. WILKERSON. 1998. Silicate regulation of new production in the equatorial Pacific upwelling. Nature **391:** 270–273.

FARRELL, J. W., T. F. PEDERSEN, S. E. CALVERT, AND B. NIELSEN.

1995. Glacial–interglacial changes in nutrient utilization in the equatorial Pacific Ocean. Nature **377:** 514–517.

FRANCOIS, R., AND OTHERS. 1997. Contribution of Southern Ocean surface-water column stratification to low atmospheric CO_2 concentrations during the last glacial period. Nature **389:** 929–935.

GOERING, J., V. ALEXANDER, AND N. HAUBENSTOCK. 1990. Seasonal variability of stable carbon and nitrogen isotopic ratios of organisms in a North Pacific bay. Estuar. Coast. Shelf Sci. **30:** 239–260.

GORDON, R. M., K. H. COALE, AND K. S. JOHNSON. 1997. Iron distributions in the equatorial Pacific: Implications for new production. Limnol. Oceanogr. **42:** 419–431.

HONJO, S., J. DYMOND, R. COLLIER, AND S. J. MANGANINI. 1995. Export production of particles to the interior of the equatorial Pacific Ocean during the 1992 EqPac experiment. Deep-Sea Res. **42:** 831–870.

HUTCHINS, D. A., AND K. W. BRULAND. 1998. Iron-limited diatom growth and Si:N uptake ratios in a coastal upwelling regime. Nature **393:** 561–564.

JOHNSON, K. S., R. M. GORDON, AND K. H. COALE. 1997. What controls dissolved iron concentrations in the world ocean? Mar. Chem. **57:** 137–161.

KNAUER, G. A., AND OTHERS. 1984. In situ effects of selected preservatives on total carbon nitrogen and metals collected in sediment traps. J. Mar. Res. **42:** 445–462.

KOLBER, Z. S., AND OTHERS. 1994. Iron limitation of phytoplankton photosynthesis in the equatorial Pacific Ocean. Nature **371:** 145–148.

KU, T.-L., S. LUO, M. KUSAKABE, AND J. K. B. BISHOP. 1995. Ra-derived nutrient budgets in the upper equatorial Pacific and the role of ''new'' silicate in limiting productivity. Deep-Sea Res. **42:** 179–197.

LANDRY, M. R., AND OTHERS. 1997. Iron and grazing constraints on primary production in the central equatorial pacific: An EqPac synthesis. Limnol. Oceanogr. **42:** 405–418.

LIU, K. K. 1979. Geochemistry of inorganic nitrogen compounds in two marine environments: The Santa Barbara Basin and the ocean off Peru. Ph.D. thesis, Univ. of California–Los Angeles.

———, AND I. R. KAPLAN. 1989. The eastern tropical Pacific as a source of ^{15}N-enriched nitrate in seawater off southern California. Limnol. Oceanogr. **34:** 820–830.

MARTIN, J. H., AND OTHERS. 1994. Testing the iron hypothesis in ecosystems of the equatorial Pacific Ocean. Nature **371:** 123–129.

MCCARTHY, J. J., C. GARSIDE, J. L. NEVINS, AND R. T. BARBER. 1995. New production along 140°W in the equatorial Pacific during and following the 1992 El Niño event. Deep-Sea Res. **43:** 1065–1093.

MONTOYA, J. P., AND J. J. MCCARTHY. 1995. Isotopic fractionation during nitrate uptake by phytoplankton grown in continuous culture. J. Plankton Res. **17:** 439–464.

MURRAY, J. W., E. JOHNSON, AND C. GARSIDE. 1995. A U.S. JGOFS process study in the equatorial Pacific (EqPac): Introduction. Deep-Sea Res. **42:** 275–293.

NAKATSUKA, T., N. HANDA, AND E. WADA. 1991. Nitrogen isotope ratio of particulate organic matter and seasonal change of nutrient budget in surface mixed layer of subarctic Pacific Ocean. I. Spatial variation of suspended particles in surface water. Deep-Sea Res. **39:** 1–33.

OWENS, N. J. P., AND A. P. REES. 1989. Determination of nitrogen-15 at sub-microgram levels of nitrogen using automated continuous-flow isotope ratio mass spectrometry. Analyst **114:** 1655–1657.

PEÑA, M. A., W. G. HARRISON, AND M. R. LEWIS. 1992. New production in the central equatorial Pacific. Mar. Ecol. Prog. Ser. **80:** 265–274.

PENNOCK, J. R., D. J. VELINSKY, J. M. LUDLAM, J. H. SHARP, AND M. L. FOGEL. 1996. Isotopic fractionation of ammonium and nitrate during uptake by *Skeletonema* costatum: Implications of $\delta^{15}N$ dynamics under bloom conditions. Limnol. Oceanogr. **41:** 451–459.

SIGMAN, D. M., M. A. ALTABET, D. C. MCCORKLE, R. FRANCOIS, AND G. FISHER. 1999. The $\delta^{15}N$ of nitrate in the Southern Ocean: II. Consumption of nitrate in surface waters. Global Biogeochem. Cycles **13:** 1148–1149.

———, ———, ———, ———, AND ———. 2000. The $\delta^{15}N$ of nitrate in the Southern Ocean: I. Nitrogen cycling and circulation in the ocean interior. J. Geophys. Res. **105:** 19,599–19,614.

———, ———, R. MICHENER, D. C. MCCORKLE, B. FRY, AND R. M. HOLMES. 1997. Natural abundance-level measurement of the nitrogen isotopic composition of oceanic nitrate: An adoption of the ammonia diffusion method. Mar. Chem. **57:** 227–242.

SMITH, C. R., D. J. HOOVER, S. E. DOAN, R. H. POPE, D. J. DEMASTER, F. C. DOBBS, AND M. A. ALTABET. 1996. Phytodetritus at the abyssal seafloor across 10° of latitude in the central equatorial Pacific. Deep-Sea Res. **43:** 1309–1338.

SUNDA, W. G., AND S. A. HUNTSMAN. 1995. Iron uptake and growth limitation in oceanic and coastal phytoplankton. Mar. Chem. **50:** 189–206.

TAKEDA, S. 1998. Influence of iron availability on nutrient consumption ratio of diatoms in oceanic waters. Nature **393:** 774–777.

TOGGWEILER, J. R., AND S. CARSON. 1995. What are upwelling systems contributing to the ocean's carbon and nutrient budgets?, p. 337–360. *In* C. P. Summerhayes, K. C. Emeis, M. V. Angel, R. L. Smith, and B. Zeitzschel [eds.], Upwelling in the ocean: Modern processes and ancient records. Wiley.

TSUCHIYA, M., R. LUKAS, R. A. FINE, E. FIRING, AND E. LINSTROM. 1989. Source waters of the Pacific equatorial undercurrent. Prog. Oceanogr. **23:** 101–147.

WADA, E. 1980. Nitrogen isotope fractionation and its significance in biogeochemical processes occurring in marine environments, p. 375–398. *In* E. D. Goldberg and Y. Horibe [eds.], Isotope marine chemistry. Uchida Rokakuho.

———, AND A. HATTORI. 1978. Nitrogen isotope effects in the assimilation of inorganic nitrogenous compounds by marine diatoms. Geomicrobiol. J. **1:** 85–101.

WASER, N. A. D., P. J. HARRISON, B. NIELSON, S. E. CALVERT, AND D. H. TURPIN. 1998. Nitrogen isotope fractionation during the uptake and assimilation of nitrate, nitrite, ammonium, and urea by a marine diatom. Limnol. Oceanogr. **43:** 215–224.

WELLS, M. L., G. K. VALLIS, AND E. A. SILVER. 1999. Tectonic processes in Papua New Guinea and past productivity in the eastern equatorial Pacific Ocean. Nature **398:** 601–603.

WU, J., S. E. CALVERT, AND C. S. WONG. 1997. Nitrogen isotope variations in the subarctic northeast Pacific: Relationships to nitrate utilization and trophic structure. Deep-Sea Res. **44:** 287–314.

WYRTKI, K. 1981. An estimate of equatorial upwelling in the Pacific. J. Phys. Oceanogr. **11:** 1205–1214.

Received: 13 July 1999
Accepted: 30 August 2000
Amended: 1 November 2000